Critical adsorption in a well-defined geometry

R. Garcia, S. Scheidemantel, K. Knorr,* and M. H. W. Chan
Physics Department, The Pennsylvania State University, 104 Davey Laboratory, University Park, Pennsylvania 16801, USA
(Received 26 June 2003; published 20 November 2003)

A fluid's density profile near a wall is predicted to assume a universal shape near the liquid-vapor critical point, a phenomenon termed critical adsorption. This universal shape is predicted to depend on the boundary conditions of the fluid at the walls and is predicted to be a function of the ratio z/ξ, where z is the distance from the wall and ξ is the bulk correlation length. A body of evidence confirms the analogous phenomenon of critical adsorption in binary fluids near the critical demixing point, but in the simple liquid-vapor system the experimental situation is not as clear. For example, critical adsorption of SF_6 was observed in porous glass for reduced temperature $t=T/T_c-1>10^{-3}$. However, for $t<10^{-3}$ a desorption behavior is seen. This desorption has so far resisted rigorous theoretical explanation. We report measurements of the critical adsorption of nitrogen inside a capacitor gap with a simple parallel plate geometry and open gap of 3 μm. Unlike the previous experiments with SF_6, the data show a monotonic increase in the adsorption between $t=5\times10^{-4}$ and $t=10^{-6}$, consistent with theoretical prediction and without any indication of desorption.

DOI: 10.1103/PhysRevE.68.056111 PACS number(s): 05.70.Jk, 64.60.Fr, 68.35.Rh, 75.40.−s

I. INTRODUCTION

The effect of a solid boundary on a simple fluid or binary fluid undergoing a continuous phase transition [1] was studied by Fisher and de Gennes [2]. Next to a *strongly* adsorbing boundary, they predicted that the order parameter profile should decay away from the boundary as

$$\rho(z)-\rho_c=Mt^{\beta}P(z/\xi,ht^{-\Delta}), \tag{1}$$

where $\rho(z)$ is the density a distance z from the boundary, ρ_c is the critical density, $t=T/T_c-1$ is the reduced temperature, $\xi=\xi_o|t|^{-\nu}$ the bulk correlation length, $\Delta=1.65$ is the gap exponent, and $h=[\mu(\rho,T)-\mu(\rho_c,T)]/2k_BT$, where $\mu(\rho_c,T)$ is the chemical potential along the critical isochore [2]. The scaling function $P(x,y)$ has a different functional form above and below T_c and is determined by the universality class of the phase transition and the boundary condition of the order parameter at the solid boundary. Equation (1) is obtained by taking the derivative with respect to h of the fundamental renormalization group scaling relation for the free energy [2]. Below T_c, $P(x,y)$ satisfies the constraint that, for $z\to\infty$ and $h\to0$, the shape of the coexistence region in the bulk is described by $\rho(z)-\rho_c=M|t|^{\beta}$, and hence $P(x,y)\to1$. Above T_c, for $z\to\infty$ and $h\to0$, it must be $P(x,y)\to0$ so that $[\rho(z)-\rho_c]\to0$.

In our experiment, the order parameter profile near the wall is not directly measurable. More relevant to our measurement is the total excess adsorption per unit area, which for a parallel plate capacitor geometry is defined by

$$\Gamma_c=\frac{1}{2}\int_0^L[\rho(z)-\rho_c]dz, \tag{2}$$

the integral being taken over the whole capacitor gap, the factor of $\frac{1}{2}$ due to the fact that the capacitor is comprised of two electrode surfaces a distance L apart. Substituting Eq. (1) in Eq. (2), we obtain

$$\Gamma_c=AM\xi_o t^{\beta-\nu}+B, \tag{3}$$

where A and B are parameters that depend on the limits of integration. The parameter B takes into account the excess adsorption due to the compression of the nitrogen by the substrate van der Waals forces, which happens even for $t\to\infty$. We estimate that B is at most 1×10^{-2} mmol/m^2, i.e., approx two solid layers. This is comparable to the noise in our measurement of Γ_c. The theoretical prediction for $h=0$ and an ideally flat substrate is $A=2.0(\pm0.5)$ [3], independent of the substrate composition so long as the attraction between substrate and fluid is strong enough to force a liquidlike layer immediately next to the wall. This prediction does not take into account the roughness of the electrodes nor the long-ranged van der Waals field that extends into the fluid from the electrodes; these can be expected to increase Γ_c (and therefore A) but they are not expected to affect the power law temperature dependence in Eq. (3) [4]. The power law dependence is expected to break down as $t\to0$ under two circumstances. First, Γ is predicted to saturate at a finite value as $t\to0$ when $\xi\gtrsim L$ because the adsorptions on the two electrode surfaces begin to interfere with each other [5]. Second, A should become temperature dependent when $h\neq0$, i.e., when the bulk fluid density next to the capacitor gap, ρ_{bulk} is no longer exactly ρ_c; this is a direct consequence of the scaling law [Eq. (1)] but has not been shown to be measurable under realistic conditions [5].

Binary fluid mixtures near their critical demixing point belong to the same universality class as the liquid-vapor critical point. Ellipsometric measurement of the volume fraction gradients in binary fluids provides significant evidence for Eq. (1), where, instead of ρ, the volume fraction of a given component v is the appropriate order parameter [3,6]. In pure fluids, by contrast, the experimental situation has

*Permanent address: Universität des Saarlandes, Saarbrücken, Germany.

been less clear. Measurements of the adsorption of SF_6 in porous glasses confirm critical adsorption above T_c for $t > 10^{-3}$ but give the opposite result, critical *desorption*, for $t < 10^{-3}$ [7]. So far, no one knows the precise cause of the observed desorption phenomenon. It has been suggested that an effective bulk field h, in addition to the surface field that ordinarily causes critical adsorption, might be responsible. Since the compressibility diverges faster than critical adsorption, the response to a bulk field tends to dominate sufficiently close to T_c, potentially leading to desorption [5]. It is not at all apparent, however, that this scenario pertains to the experiment of Ref. [7] since in their experiments the chemical potential is not fixed but varies with temperature. A simulation of a Lennard-Jones fluid confined inside a gap with simple parallel plate geometry, which is meant to closely mimic the experiment of Ref. [7], including the effect of nonzero h, does not show any evidence of desorption [5]. Thommes *et al.* [7] have suggested that the desorption could be related to the confinement of the critical fluctuations in the pores, since the onset of desorption occurred when the correlation length ξ became much larger than the 20–30 nm substrate pore diameter. If the pore size in relation to ξ is so important, however, it is difficult to explain why the same temperature dependence of the desorption is observed for the adsorption of SF_6 in finely divided graphitized carbon black (Vulcan 3G). In Vulcan 3G, the distances between the exposed surfaces of neighboring particles are distributed widely, with a typical distance of 5–10 nm [8].

In this paper, we report experimental measurement of the critical absorption of nitrogen inside a capacitor gap with a simple parallel plate geometry and open gap $L = 3\ \mu$m. The value Γ_c deduced from the capacitance data is consistent with theoretical prediction, for t between 3×10^{-6} and 4×10^{-4} and reduced density $\rho^* = \rho/\rho_c - 1$ between -0.04 and 0.007. While we observe, as expected [5], that the adsorption saturates below $t = 3 \times 10^{-6}$, we do not see any hint of desorption in the data.

II. EXPERIMENTAL CELL

In Fig. 1(a) we show the schematic of the experimental cell. During the measurements, the cell is completely filled with fluid N_2. Inside the cell, there are three electrodes comprising two capacitors. Electrodes A and B are machined out of Cu and polished using diamond paste to a mirrorlike finish. Electrode B, which is shaped like a cylinder, fits snuggly inside the annulus-shaped electrode A. Electrode C consists of a circular 10-μm-thick kapton diaphragm that is stretched and glued onto a copper ring. The kapton is plated with aluminum on the side facing electrode B and it is perforated away from the active region near electrode B to assist diffusive equilibrium in the cell. All the electrodes have a mirrorlike finish but contain scratches and other imperfections that remain visible to the naked eye over about 1% of the active area. Capacitor AC, which has a gap of 260 μm, is used to measure the density of the bulk fluid. Capacitor BC, with a much smaller gap of 3.0 μm, is expected to be much more sensitive to critical adsorption effects. For example, when $t \sim 10^{-6}$, critical adsorption is expected to produce a $\sim 1\%$ increase in average ρ/ρ_c within capacitor BC but only a $\sim 0.01\%$ increase within capacitor AC.

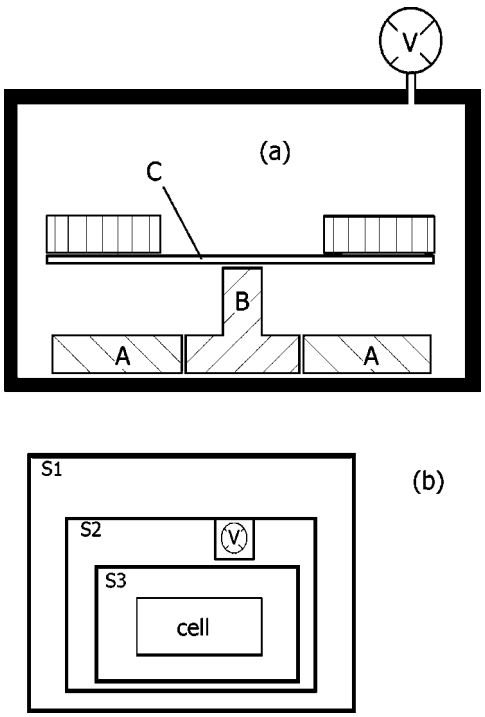

FIG. 1. (a) Schematic drawing of the Cu experimental cell showing three electrodes A, B, and C, not drawn to scale. Capacitor AC, which has a gap of 260 μm, is used to measure the bulk fluid, while capacitor BC, with a gap of 3.0 μm, is sensitive to critical adsorption effects. A tilt in the cell of only 2° would be enough so that capacitor BC is situated very close to capacitor AC. (b) Schematic of the cryostat showing three temperature control stages S1 (regulated at 77 K), S2 (regulated at 126 K), S3 (floating), low temperature valve V (regulated at 129 K), and experimental cell.

Because electrode C consists of a flexible, kapton diaphragm, it would be expected to deflect in response to the temperature-dependent fluctuation-induced critical Casimir force [17], potentially obfuscating our measurement of the density increase due to critical adsorption between electrodes B and C. Another potential source of error in our measurement is an increase in the density inside the capacitor gap due to electrostriction [9]. We find, however, that these two effects produce a negligible correction in the measured adsorption.

The kapton which comprises electrode C is stretched so tightly upon cooling from room temperature that it is essentially flat and insensitive to the various forces that are present. We measured the deflection of the kapton diaphragm in response to a varying applied ac voltage across the gap, obtaining coefficient of sensitivity of the diaphragm $\beta = 1.7 \times 10^{-10}$ m^3/N that relates the deflection of the diaphragm Δd to the pressure ΔP acting on it, i.e.,

$$\Delta d = \beta \Delta P. \tag{4}$$

Based on this calibration, the critical Casimir pressure [2,10] $\sim F k_B T_c / d^3$ should produce a fractional change in the capacitance of less than 3×10^{-7}, even after taking into ac-

count a predicted enhancement of the force near the critical point $F<100$ [10]. This is completely negligible compared to the 0.1% increase in the capacitance of capacitor BC due to the 1% increase in ρ/ρ_c due to critical adsorption.

The electrostatic pressure due to an applied ac voltage V is given by $\Delta P=[\frac{1}{2}\varepsilon_o[(V-Vo)/d]^2$, where ε_o is the electric permittivity, d is the capacitor gap, and V_o is the dc voltage drop due to contact potentials in the circuit. During the measurements, the maximum ac voltage across capacitor BC is 5 mV, while the maximum voltage across capacitor AC is 80 mV. The dc voltage drop is found to be $V_o \sim 24$ mV. We did not do anything to try to compensate for V_o because the effect of the dc field is so small. In the worst case, when $t\sim 10^{-6}$, the expected electrostrictive increase in the density [9] inside the capacitor gaps due to ac and dc fields is only 0.01% in capacitor BC and 0.0001% in capacitor AC. When $t\sim 10^{-4}$, the increase in the density is only 4×10^{-5}% in capacitor BC and 4×10^{-7}% in capacitor AC. An increase of 0.01% in the density is less than the scatter in our measurement of critical adsorption.

The most important obfuscating effect in our experiment is due to gravity which induces a gradient in the density as a function of height inside the cell [11]. As $T\rightarrow T_c$, because of the fluid's diverging compressibility, gravity progressively increases the density of the supercritical fluid in the lower half of the cell, where both capacitors AC and BC are located. When $t\sim 10^{-6}$, the gravity-induced increase in the density in these capacitors is measured to be about 4%, at least four times larger than the increase in density inside capacitor BC expected due to critical adsorption. In our analysis, we ''subtract out'' the density increase observed in capacitor AC from the data of capacitor BC. The basis of this ''subtraction'' is the assumption that the density of the bulk fluid next to capacitor BC is the same as the average density measured by capacitor AC. For $t>10^{-5}$, this assumption works for the various densities studied in this experiment, the error due to the density gradient within capacitor AC being comparable to the noise in our measurement. For this reason, we restrict the power law analysis of our data to $t>10^{-5}$. Closer to the critical point, for $t<8\times 10^{-6}$ and $|\rho^*|<0.01$, the density gradient within capacitor AC is expected to become sufficiently pronounced that capacitor AC measures a ''rounded'' density and there is a measurably significant density difference between the bulk next to capacitor BC and at the center of capacitor AC. This rounding and density difference are sensitive to the precise leveling of the experimental cell, which we do not have the means of determining at low temperature. A tilt in the cell of 2° is within our experimental uncertainty, especially if we consider the possible effect due to differential thermal contraction during the cooldown. The cell schematic in Fig. 1(a), showing capacitor BC at a height above 99% of the fluid in capacitor AC, refers to the very unrealistic case in which we would be able to make the cell perfectly horizontal. A tilt of 2° would result in capacitor BC being below 40% of the fluid in capacitor AC, effectively much closer to the center of capacitor AC, reducing the error due to the gradient in density within capacitor AC.

III. EXPERIMENTAL PROCEDURE

Our measurements consist of a series of experimental runs where, for each run, we first adjust the average density inside the cell in the one-phase region above T_c. Then we perform two data runs back to back. First, we measure as a function of temperature C_{AC}, the capacitance between electrodes A and C. Second, we measure the ratio C_{BC}/C_{AC} as a function of temperature, where C_{AC} is the capacitance between electrodes A and C and C_{BC}, the capacitance between electrodes B and C.

In Fig. 1(b), we show a schematic of the cell, the various shields, and thermally controlled stages. Calibrated Pt thermometers are used to measure the temperature of shield S2, the low temperature valve V, and the cell. Shield S1 consists of the vacuum can which is submerged in liquid nitrogen (77 K). A Lakeshore resistance bridge controller [12] regulates the temperature of S2 at ~ 126 K(± 1 mK). An LR-700 resistance bridge controller [13] regulates the temperature of V at 129 K(± 1 mK). The shield S3, which isolates the cell from S2 and V, is left unregulated and floats at a temperature intermediate between that of S2 and V. To obtain greater sensitivity and lower noise in our measurement of the cell thermometer, it is measured using a homemade low current 4-lead ac resistance bridge with standard resistor bolted onto the cell [14]. Because the cell is suspended from S3 using thin stainless steel capillary with low thermal conductivity, the heating and cooling of the cell is almost completely due to thermal radiation between it and S3. The time constant of the cell's response to a change in the temperature of S2, which is about 1 day, is determined by the large heat capacity due to the thick-walled Cu cell and the weak thermal link to S3.

Because of the large thermal time constant of the cell, we allow the cell temperature to drift through T_c, rather than control the temperature at each point. We quickly lower the temperature below T_c at the start of each data run and then let the cell drift up slowly at ≈ 2.5 mK/hr. This drift rate is comparable to that used in previous experiments near critical points [15]. Because of the thick walls of the Cu cell and the high thermal conductivity of Cu, the temperature gradient in the walls of the cell is negligible, but we need to consider the temperature gradient between the cell walls and the nitrogen fluid. When we compared two data runs in which the cell was allowed to drift much faster at ± 15 mK/hr both up and down in temperature, a discrepancy of 3 mK was observed in the two curves near the critical point. To estimate the maximum likely magnitude of the error for the actual drift rates used in the critical adsorption measurements, we compared data obtained from nearly identical runs that approached very close to the critical point, simultaneously within $t<10^{-6}$ and $\rho^*<10^{-4}$, but with different drift rates (3.5 mK/hr vs. 2.5 mK/hr). We observed a discrepancy in the two datasets on the order of 0.3 mK, only somewhat larger than the scatter. Based on this information, we estimate an error in t of at most 2×10^{-6} for the 2.5 mK/hr drift rate used.

IV. CAPACITANCE DATA FOR LARGE GAP CAPACITOR

Figure 2(a) shows C_{AC}, the capacitance between electrodes A and C as a function of temperature, measured using

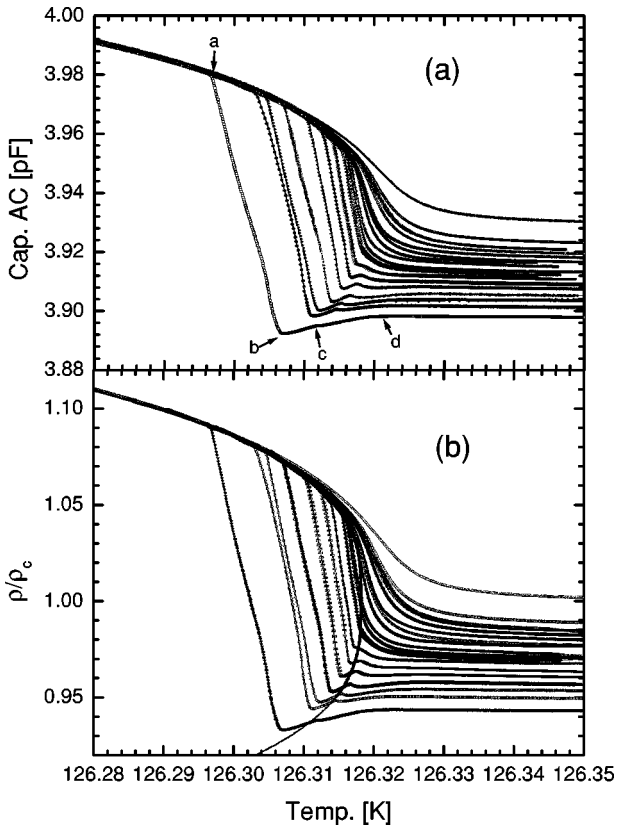

FIG. 2. (a) Capacitance between electrodes A and C as a function of temperature. For clarity, not all of the data, which extend down to 125.9 K, are shown. The absolute uncertainty in the temperature scale is about 0.1 K based on the thermometer calibration, while the uncertainty in the capacitance is about $\pm 4\times 10^{-6}$ pF. (b) Density calculated from data of panel (a) using the Clausius-Mossotti relation. The solid curve corresponds to the bulk coexistence curve.

an Andeen-Hagerling capacitance bridge [16] operating at 1000 Hz. Electrode B is grounded during this measurement. The various curves correspond to different fillings or average densities in the cell. For $T \ll T_c$, i.e., below point *a* in Fig. 2(a), the curves collapse onto a single capacitance curve whose temperature dependence reflects the temperature dependence of the bulk liquid density. This happens because capacitor AC is in the lower half of the cell, so that, at sufficiently low temperature, it is located below the level of the liquid miniscus. As the temperature of the cell is increased, eventually the liquid level drops below the level of electrode C so that the measured density no longer follows the liquid side of the coexistence curve but instead drops off approximately linearly with T as the capacitor empties of liquid. When the liquid level in the cell drops below the level of electrode A, capacitor AC is then completely in the vapor phase but there is still a liquid layer adsorbed onto the electrodes. Consequently, the temperature dependence of the capacitance between points *b* and *c* in Fig. 2(a) does not precisely follow the temperature dependence of the vapor density in this region. As the liquid level drops further and further inside the cell, the liquid layer adsorbed onto the electrodes progressively thins, so that the measured density more closely approximates the vapor density. Then, precisely at the vapor side of the coexistence boundary, point *c* on the lowest curve in Fig. 2(a), there is a downward kink in the capacitance. The capacitance drops off and then increases between points *c* and *d*. This curious behavior at the lower coexistence boundary is a consequence of the gravity-induced density gradient. The density of the fluid increases as we go lower down in the cell, so that at some point near the bottom of the cell the density is sufficiently high that a puddle of liquid is formed. The formation of this puddle has the effect of decreasing the average density of the rest of the fluid in the cell and this is reflected, in particular, in the lower density of the vapor measured by capacitor AC. Above T_c (above point *d*), there is no more liquid present anywhere in the cell, but C_{AC} is nevertheless observed to vary due to the aforementioned gravity-induced compression of the supercritical fluid. As the temperature is increased further still the capacitance curves flatten out and their value now reflects the total average density of the fluid in the cell.

Figure 2(b) shows ρ/ρ_c, the density normalized by the critical density, calculated from the data of Fig. 2(a) using the Clausius-Mossotti relation

$$\frac{\varepsilon-1}{\varepsilon+2}=\frac{4\pi\alpha}{3}\frac{\rho}{\rho_c}, \tag{5}$$

where $\alpha=1.175\,272\times10^{-2}$ is the atomic polarizability of nitrogen in dimensionless units [14]. In this equation, the effective dielectric constant $\varepsilon=C/C_o$, where C is the measured capacitance and C_o is the empty capacitance. The critical point is where on the coexistence curve the slope is vertical, and corresponds to $\rho=\rho_c$ and $T=T_c$. We fit C_o by requiring at $\rho=\rho_c$ that $\varepsilon=\varepsilon_c=1.155\,336$ [14]. Also in the figure, we show the bulk coexistence curve from Ref. [14],

$$\rho/\rho_c=1+0.717\,46|t|\pm1.520|t|^{0.327}(1+1.03|t|^{0.51}-2.0|t|^{2\times0.51}). \tag{6}$$

The $\pm$ refers to the liquid or vapor side of the coexistence curve. The various exponents and coefficients are taken from Ref. [14], where 0.327 and 0.51 are the asymptotic and correction to scaling exponents. However, we obtain the width $M=1.520\pm0.001$ and $T_c=126.3182\pm0.0002$ instead of $M=1.479\pm0.006$ and $T_c=126.2143\pm0.0002$ obtained by Ref. [14]. The differences in T_c are most likely due to an inconsequential difference in thermometer calibration. The width M obtained in this experiment is closer to the cubic model value $M=1.59$ [11].

V. CAPACITANCE DATA FOR THE SMALL GAP CAPACITOR

Figure 3(a) shows the ratio C_{BC}/C_{AC}, as measured by a standard ac ratio bridge circuit [14]. By measuring this ratio rather than individual capacitances directly, we are able to minimize the error due to temperature drift rates that varied slightly from run to run. Between different runs, when we disconnect and reconnect the circuits, we observed shifts in

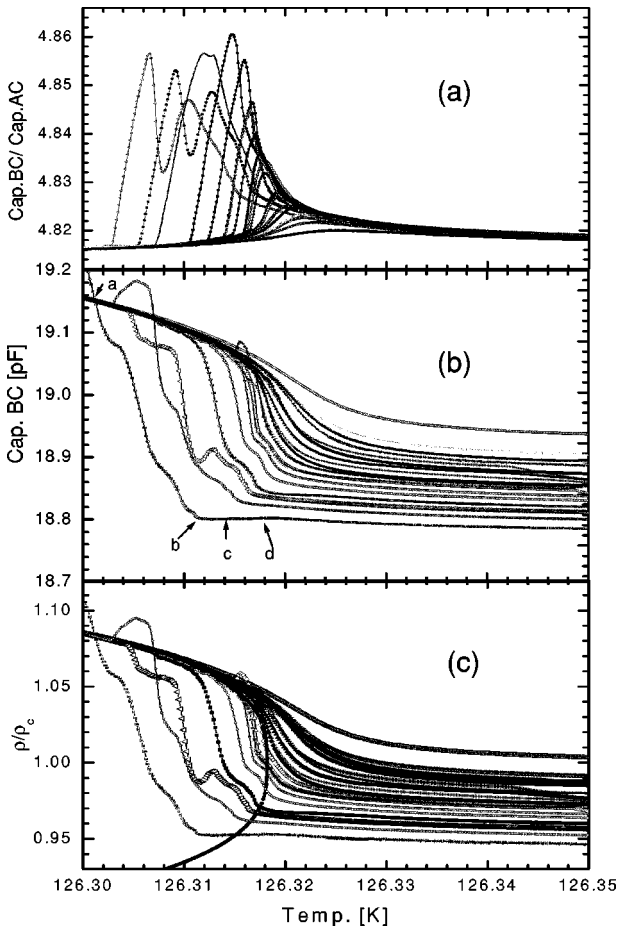

FIG. 3. (a) Ratio of the capacitance between electrodes B and C to the capacitance between electrodes A and C measured by our bridge circuit. (b) Capacitance between electrodes B and C as a function of temperature, determined by multiplying the data of Figs. 2(b) and (a). The uncertainty in the vertical scale is $\pm 2.7 \times 10^{-2}$ pF. (c) Density calculated from data of panel (b). The solid curve corresponds to the same bulk coexistence curve shown in Fig. 2(b).

the measured ratio, which correspond to shifts as much as 2.7×10^{-2} pF in C_{BC}. These shifts may be due to stray capacitances in our circuit and possible small irreproducibilities in the adjustment of the phase in the lock-in amplifier used in the ac ratio bridge. To correct for these shifts, since the dielectric constant data (and therefore the ratio) must collapse for $T \ll T_c$ we adjusted all the data so that they collapse in this region.

In Fig. 3(b), we show C_{BC}, which we obtain by multiplying together C_{AC} from Fig. 2(b) and C_{BC}/C_{AC} from Fig. 3(a). In Fig. 3(c), we show the effective density in capacitor BC calculated from the data of Fig. 3(b) using Eq. (5) and $C_o = 16.382$ pF. This value of C_o is obtained by requiring that the dielectric constant at temperatures far below T_c matches that of the bulk liquid. The solid line in the figure indicates the same bulk coexistence region which we indicated in Fig. 2(b).

There are several significant differences between the data of Figs. 3(c) and 2(b). These differences are especially striking below T_c. For example, along the vapor side of the coexistence curve, between points *b* and *c* in the figure, the effective density shown in Fig. 3(c) deviates much more significantly from the expected density due to the vapor. This more pronounced deviation is because the liquid film adsorbed on the electrodes makes a greater contribution to the capacitance of the small gap capacitor. In Fig. 3(c), we also note that the calculated effective density of some of the curves shows a peaklike anomaly where the calculated effective density actually exceeds the bulk liquid density. This anomaly is mostly likely caused by the presence of a metastable liquid droplet on top of electrode C, whose weight would cause the kapton diaphragm to sag, reducing the size of the gap, and giving a peaklike anomaly in the capacitance. The apparent peak in the effective density in Fig. 3(c) is then an artifact due to our assumption that the gap did not change when we calculate the effective density. The most interesting difference between Figs. 3(c) and 2(b) is in the region just above the vapor side of coexistence curve, e.g., between points *c* and *d* for the bottom curves in the two figures. In these regions, the data of Fig. 2(b) typically show a dip in the effective density, due to gravitationally induced decrease in the vapor density, but the data of Fig. 3(c) do not. This difference, we think, is due to critical adsorption onto the capacitor surfaces, which in the case of capacitor BC compensates almost exactly for the effect of gravity-induced gradients in the cell.

VI. ANALYSIS

In our analysis, we make use of data in the region below T_c, between 125.9 K and 126.2 K, to determine the locus of the critical temperature and critical density, but, our main interest is the region above T_c, where no liquid is present anywhere in the cell. While Eqs. (1) and (2) should apply both above and below T_c, too many unknowns exist in our experiment just below T_c to allow for a quantitative test. For example, below T_c we expect critical adsorption at both the vapor-liquid and the liquid-substrate interfaces, but we do not have a way of separating the two effects. We also do not have a way of determining the density of the liquid film adsorbed on the electrodes and we do not know the precise position of the bulk liquid level in the cell as a function of T which ultimately determines the thickness of the adsorbed film. Finally, below T_c we notice that sometimes liquid droplets appear to linger on electrode C, causing an anomaly in some of the curves in Fig. 3(c). By contrast, above T_c we expect no such spurious effects and there are no problems due to liquid being formed at the bottom of the cell.

Above T_c, Eq. (3) assumes there is no gravity present so that the density of the bulk fluid at the same height as the capacitor is constant, an increase in the capacitance occurring due to only critical adsorption as $t \to 0$. However, in our experiment the density of the bulk fluid at the position of capacitor BC also increases due to gravity. In particular, we note that in both Figs. 2 and 3, the effective density increases as $T \to T_c$ even when $T > T_c$. For capacitor AC, the increase in the density is almost completely due to gravity, the increase due to critical adsorption being less than 0.01%. For capacitor BC, which has a much smaller gap, the increase

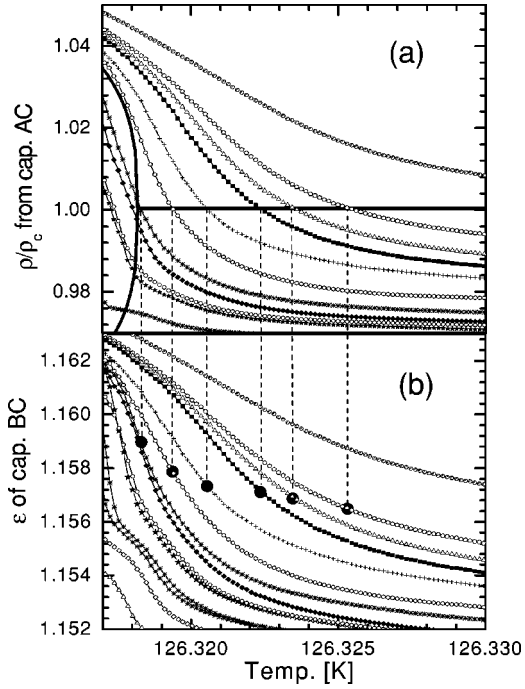

FIG. 4. (a) A blowup of the effective density of capacitor AC in the region just above $T_c = 126.3182$ K in Fig. 2(b). (b) The effective dielectric constant for capacitor BC, ε_{BC}, calculated from the data of Fig. 3(b). Each curve in panel (b) corresponds to a curve in panel (a) taken under identical conditions with the same average density inside the experimental cell. The thick solid line in panel (a) corresponds to the critical density. Where this line intersects a data curve in Fig. 4(a) corresponds to a point where the average density of the bulk fluid in capacitor AC is constant and equal to ρ_c. Each of these points corresponds to a point on a data curve in panel (b), e.g., denoted by a dark circle. The increase in ε_{BC}, even while the density in capacitor AC is constant, is due to critical adsorption.

due to gravity and critical adsorption are comparable in magnitude. Because capacitor BC is located close to the center of gravity of capacitor AC, the density deduced from C_{AC} gives the density of the bulk fluid at the same height at capacitor BC, at least for $t > 10^{-5}$. As a result, by using both the C_{AC} and C_{BC} data, we can separate out the effects due to gravity and critical adsorption.

Figure 4 shows a blowup of the data in the region above T_c. Figure 4(a) shows the density calculated from C_{AC} (the large gap capacitor) and Fig. 4(b) shows the effective dielectric constant for C_{BC} (the small gap capacitor). For each curve in Fig. 4(a) there is a corresponding curve in Fig. 4(b) taken under identical conditions with the same average density inside the experimental cell. The thick horizontal line in Fig. 4(a) represents a constant density cut of $\rho = \rho_c$. The point where this line intersects a particular data curve in Fig. 4(a) corresponds to the temperature on that curve where the average density of the bulk fluid in capacitor AC is equal to ρ_c. For each point in Fig. 4(a) intersecting $\rho = \rho_c$, there is a point on a corresponding data curve in Fig. 4(b) denoted by a dark circle. In Fig. 4(b), the increase in the dielectric constant of the small gap capacitor BC as T is reduced towards T_c, even while the density in the large gap capacitor AC is constant, is due to critical adsorption.

We can relate the effective dielectric constant ε of a parallel plate capacitor to Γ_c [Eq. (2)] in a simple way. From the law for adding capacitances in series,we have for a gap of dimension L,

$$L/\varepsilon = \int_0^L dz/\varepsilon(z). \tag{7}$$

Substituting for $\epsilon(\Delta\rho/\rho_c)$ in Eq. (7) and in performing a Maclaurin series expansion, where we retain terms linear $\Delta\rho/\rho_c$, gives

$$\Gamma_c = \frac{0.950\,77\rho_c L\varepsilon_c^2}{2(\varepsilon_c - 1)}\left(\frac{1}{\varepsilon_c} - \frac{1}{\varepsilon}\right), \tag{8}$$

where, as before, $\varepsilon_c = 1.155\,336$ is the dielectric constant at critical density. Even though the density of the bulk fluid may reach the solid density near the wall, $\Delta\rho/\rho_c \sim 2$, we find for the temperature range of our experiment that the various approximations used to obtain Eq. (8) introduce at most 5% error in the integral Γ_c. Note that in Eq. (8) ε refers to the effective dielectric constant due to the fluid inside the capacitor with small gap L, which is not the same as ε_{BC}. From Fig. 1, we see that capacitor BC is comprised of a large gap capacitor in parallel with a small gap capacitor. When the cell is empty, the field due to the large gap contributes 1.60 pF in parallel with 14.782 pF due to the small gap. Knowing this, from the law of adding capacitances in parallel, we obtain

$$\varepsilon = \varepsilon_{BC} + \frac{1.60}{14.782}(\varepsilon_{BC} - \varepsilon_{AC}),$$

where ε_{AC} is the effective dielectric constant of the large gap capacitor capacitor AC and $\varepsilon_{BC} = C_{BC}/16.382$ pF.

In Fig. 5(a) we show the total excess adsorption Γ_c obtained from our data as a function of reduced temperature t. Each curve in Fig. 5(a) corresponds to a different fixed effective density in capacitor AC and hence a different horizontal path in Fig. 4(a). In Fig. 5(a) the various curves do not collapse along the vertical because in the definition of Γ_c [Eq. (3)] we substract ρ_c not ρ_{bulk}. As can be seen in Fig. 5(b), if we plot instead the corresponding Gibbs absorption

$$\Gamma_{Gibbs} = \frac{1}{2}\int_0^L (\rho - \rho_{bulk})dz = \Gamma_c + \frac{1}{2}\int_0^L (\rho_c - \rho_{bulk})dz,$$

all the data collapse on each other within the scatter.

In the Introduction, we noted two factors that potentially would be expected to make the data in Fig. 5(b) not collapse as $t \to 0$: large gravity-induced density gradients that develop inside capacitor AC and the temperature dependent A in Eq. (3) due to nonzero h. The effects due to both these factors depend on the magnitude of ρ^*. The remarkably good col-

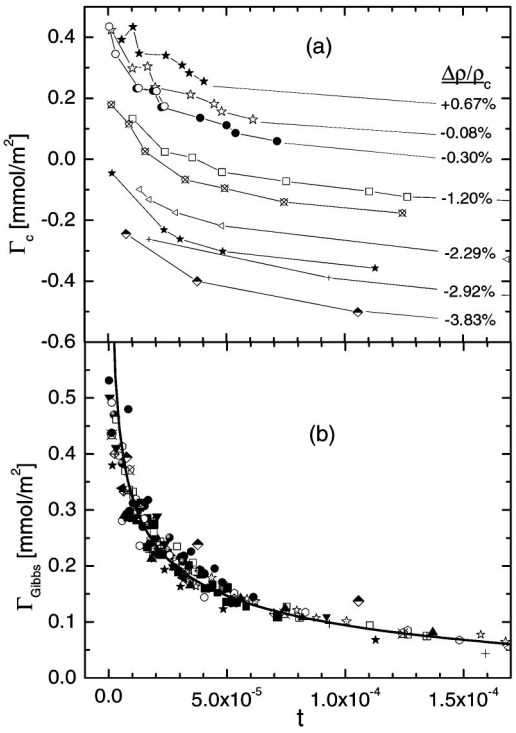

FIG. 5. (a) Total excess adsorption Γ_c calculated using the dielectric constant data of Fig. 3(b) together with the data of Fig. 2(b). Each curve corresponds to a different constant effective density in capacitor AC, where $-0.038<\Delta\rho/\rho_c<0.007$. For clarity, only about one out of four data curves are shown. (b) Total Gibbs adsorption Γ_{Gibbs} calculated from the data of panel (a). While the scatter in Γ_{Gibbs} is only ± 0.05 mmol/m^2, there is an absolute uncertainty of ± 0.16 mmol/m^2 in the vertical scale due to the uncertainty in C_{BC}. The uncertainty in t is $\pm 2\times 10^{-6}$ due to an uncertainty in T_c of ± 0.2 mK.

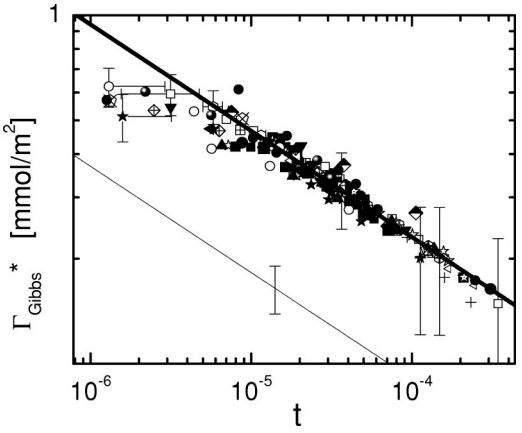

FIG. 6. Γ_{Gibbs}, from Fig. 5(b) corrected by adding 0.133 mmol/m^2 as discussed in the text. The solid line is a least-squares fit to the data above $t=10^{-5}$ also shown in Fig. 5(b). The vertical error bars reflect an experimental uncertainty of ± 0.08 mmol/m^2. The horizontal error bars correspond to an uncertainty in T_c of ± 0.2 mK. The thin solid line is the theoretical prediction for critical adsorption.

lapse of the data in Fig. 5(b), *especially over the large range of densities* (ρ^*) *studied*, indicates that either the two sources of noncollapse are individually negligible within the scatter of our data or that they compensate each other. Because there is no estimate in the literature of the effect of nonzero h, we cannot distinguish these two effects with certainty.

It is possible that the noncollapse due to gravity-induced gradients would be negligible if the cell were slightly tilted and it is unlikely that our experimental cell is perfectly level. If by accident, the cell were perfectly level, then capacitor BC would be 130 μm higher than the center of capacitor AC as shown in Fig. 1(a). For $t<10^{-5}$ gravity would then cause a lower density in capacitor BC and therefore an apparent dip in the measured Γ_{Gibbs}. The magnitude of this dip would increase as $\rho^*\to 0$. For $t=2\times 10^{-6}$, the gravity-induced gradient for $\rho^*=-0.026$ would produce an apparent dip in Γ_{Gibbs} of 0.015 mmol/m^2 while for $\rho^*=-0.0075$ the dip would be 1.5 mmol/m^2. However, if the cell is tilted by $\sim 2°$, this would place capacitor BC very close to the center of gravity of capacitor AC, substantially reducing the error due to gravitational gradients in capacitor AC. Apart from a possible effect due to nonzero h, then, the fact that in Fig. 5(b) we do not observe ρ^*-dependent dip in Γ_{Gibbs} is evidence that the cell must be tilted to some degree.

The main result of Fig. 5 is that there is no hint of critical desorption anywhere in the data, Γ_{Gibbs} showing only a monotonic increase as $t\to 0$. The solid curve in Fig. 5(b) is a least-squares fit of the data to the power law expression $\Gamma_{Gibbs}=AM\xi_o t^{\beta-\nu}+B$. The data for $t<10^{-5}$ are shown in the various plots. However, because the uncertainty in t is $\pm 2\times 10^{-6}$ (due to an uncertainty in T_c of ± 0.2 mK), and because of uncertainties due to gravitational rounding within capacitor AC, we have excluded the data for $t<10^{-5}$ from quantitative analysis. We have also fixed the exponent at the theoretical value $\beta-\nu=-0.305$. The fit yields $AM\xi_o = 1.39(\pm 0.03)\times 10^{-5}$ mol/m^2 and $B=-0.133(\pm 0.07)$ mmol/m^2. (Due to the scatter in the data, an attempt to simultaneously obtain $AM\xi_o$, $\beta-\nu$, and B from a least-squares fit gives errors as large or larger than the fitted values.) The negative value for B is unphysical because we expect $\Gamma\to 0$ as $t\to\infty$. We are not certain if the fitted value of B has any physical significance. However, we note that its value is comparable to the uncertainty in Γ due to the shifts we noted earlier in the ratio C_{BC}/C_{AC} between different runs. The resulting uncertainty in the dielectric constant $\Delta\varepsilon_{BC} = 1.6\times 10^{-3}$ translates to an uncertainty in $\Gamma \simeq 0.1028$ mol/m$^2\times\Delta\varepsilon = 0.16$ mmol/m^2. A power law plot is shown in Fig. 6, where we have added 0.133 (± 0.07) mmol/m^2 to the data from Fig. 5(b) so that the adsorption extrapolates to zero for $t\to\infty$. For comparison, the thin solid line in Fig. 6 is the theoretical prediction, where $AM\xi_o=5.45(\pm 1.3)\times 10^{-6}$ mol/m^2, $\beta-\nu=-0.305$, and $B\sim 0$.

VII. DISCUSSION

Whereas in previous experiments critical desorption of SF_6 was seen for $t\leqslant 10^{-3}$ in porous media [7], we do not see any hint of critical desorption in any of our data. Instead, the

results are consistent with the Fisher–de Gennes prediction for strong critical adsorption [Eq. (3)] in the range $3\times10^{-6}\leqslant t\leqslant 4\times10^{-4}$. As seen in Fig. 5, the theoretical value of the critical exponent describing the adsorption is consistent with our data, but the magnitude of the adsorption is 1.5 times higher than expected. Based on previous experience with polished metal surfaces, this higher than expected magnitude may be due to an enhancement of the surface area of the electrodes due to roughness (see, for example, Ref. [17]). While roughness would increase the total adsorption inside the capacitor gap, it is predicted not to affect the temperature dependence [4]. Another possible explanation is that the extra adsorption is due to the long-ranged van der Waals forces that extend into the fluid from the substrate. However, for $t=1\times10^{-6}$ we estimate an increase in Γ_{Gibbs} of 0.02 mmol/m^2 and for $t=1\times10^{-6}$ an increase of 0.11 mmol/m^2, on the basis of a crude model taking into account the diverging compressibility of the bulk fluid near its critical point [11] and using the DLP formula for the dispersion forces between substrate and fluid [17]. These increases are comparable to the noise in our data. Although in principle electrostriction would lead to an overestimate of the true Γ_{Gibbs}, we have already noted that it is of negligible magnitude compared to critical adsorption. Other errors inherent in our experimental method cannot explain the higher than expected adsorption because they lead to an underestimate of Γ_{Gibbs}, such as the fringe field contribution to ε_{BC} and the error due to the slightly higher position of the capacitor BC relative to the center of capacitor AC.

One curious feature of the critical adsorption data in Fig. 6 is that the adsorption is observed to saturate below 3×10^{-6}. We are not sure whether this flattening out is physically meaningful because the deviation from the power law behavior is comparable to the uncertainty in the reduced temperature due to the uncertainty in the determination of T_c. However, if meaningful, this feature can be blamed in part to at least three distinct causes: gravitational rounding [11], the effect of nonzero h [5], or saturation of Γ due to $\xi\gtrsim L$.

As discussed in the Introduction, the presence of gravity complicates the analysis [11], but we corrected for gravity-induced density gradient, using the data of capacitor AC to determine when the density next to capacitor BC is approximately constant. The collapse of Γ_{Gibbs} in Figs. 5(b) and 6 for ρ^* between -0.04 and 0.007, with no systematic trend in the scatter, would seem to imply that the correction applied is adequate. As we have noted, this collapse for $t<10^{-5}$ may be a somewhat fortunate result due to a slight tilt in the cell. The effect of a temperature dependent A in Eq. (3) has not been determined. Another possibility is that the flattening out below $t=3\times10^{-6}$ is due to ξ becoming comparable to d [5] or related in some other way to the confinement of critical fluctuations [7,8]. This is supported by the observation that, for $t=10^{-6}$, $\xi=1.6\times10^{-10}t^{-0.63}\sim1$ μm, which is only three times smaller than $d\sim3$ μm.

VIII. CONCLUSIONS

Our measurements of critical adsorption of nitrogen inside a capacitor gap with a simple geometry appear consistent with the Fisher–de Gennes prediction for a strongly adsorbing boundary [2]. We do not see any critical desorption down to $t\sim10^{-6}$. As we pointed out in the Introduction, it may be that the desorption observed in previous measurements of critical adsorption in porous glasses and exfoliated graphite is associated with the confinement of critical density fluctuations [7,8]. Our present results neither confirm nor exclude this explanation for the liquid-vapor system. To resolve this issue, further measurements are desirable that can delineate these two effects. Work is presently underway to do precisely this.

ACKNOWLEDGMENTS

We thank M. Krech, M. Cole, and especially A. Maciolek and R. Evans for informative discussions. This work was supported by NASA's Office of Biological and Physical Research under Grant No. NAG8-1761.

[1] C. Domb, *The Critical Point* (Taylor & Francis, London, 1996); J. Cardy, *Scaling and Renormalization in Statistical Physics* (Cambridge University Press, Cambridge, 1996).

[2] M.E. Fisher and P.-G. de Gennes, C. R. Seances Acad. Sci., Ser. B **287**, 209 (1978).

[3] S. Dietrich, in *Phase Transitions and Critical Phenomena*, edited by C. Domb and J. Lebowitz (Academic, London, 1988), Vol. 12, p. 1; H.W. Diehl and M. Smock, Phys. Rev. B **47**, 5841 (1993); **48**, 6470(E) (1993); M. Smock, H.W. Diehl, and D.P. Landau, Ber. Bunsenges. Phys. Chem. **98**, 486 (1994); A. Ciach, A. Maciolek, J. Stecki, J. Chem. Phys. **108**, 5913 (1998); B.M. Law, Prog. Surf. Sci. **66**, 159 (2001).

[4] A. Hanke, M. Krech, F. Schlesener, and S. Dietrich, Phys. Rev. E **60**, 5163 (1999).

[5] A. Maciolek, R. Evans, and N.B. Wilding, Phys. Rev. E **60**, 7105 (1999); A. Maciolek, A. Ciach, and R. Evans, J. Chem. Phys. **108**, 9765 (1998).

[6] D. Beaglehole, J. Chem. Phys. **73**, 3366 (1980); C. Franck and S.E. Schnatterly, Phys. Rev. Lett. **48**, 763 (1982); N.S. Desai, S. Peach, and C. Franck, Phys. Rev. E **52**, 4129 (1995); G. Floter and S. Dietrich, Z. Phys. B: Condens. Matter **97**, 213 (1995); D.S.P. Smith and B.M. Law, Phys. Rev. E **54**, 2727 (1996); D.S.P. Smith *et al.*, *ibid.* **55**, 620 (1997).

[7] M. Thommes, G.H. Findenegg, and M. Schoen, Langmuir **11**, 2137 (1995).

[8] M. Thommes, G.H. Findenegg, and H. Lewandowski, Ber. Bunsenges. Phys. Chem. **98**, 477 (1994).

[9] Zimmerli *et al.*, Phys. Rev. Lett. **82**, 5253 (1999).

[10] A. Drzewinski, A. Maciolek, and R. Evans, Phys. Rev. Lett. **85**, 3079 (2000); A. Drzewinski, A. Maciolek, and A. Ciach, Phys. Rev. E **61**, 5009 (2000).

[11] M.R. Moldover *et al.*, Rev. Mod. Phys. **51**, 79 (1979).

[12] Model 340 resistance bridge, Lakeshore Cryotronics, Inc., 575 McCorkle Blvd, Westerville, OH 43082, USA.

[13] Model LR-700 ac resistance bridge, Linear Research, Inc., 5231 Cushman Place, Suite 21, San Diego, CA 92110, USA.
[14] M. Pestak and M.H.W. Chan, Phys. Rev. B **30**, 274 (1984).
[15] R. Allen Willkinson *et al.*, Phys. Rev. E **57**, 436 (1998).
[16] Model 2500A electronic ac capacitance bridge, Andeen-Hagerling, Inc., 31200 Bainbridge Rd., Cleveland, OH 44139, USA.
[17] R. Garcia and M.H.W. Chan, Phys. Rev. Lett. **83**, 1187 (1999).